

Galilean Spyglass Learning Project

Julien¹

Contents

1	Summary	2
2	Requirements	2
3	Materials	2
4	Optics	3
4.1	Optic Studio Design	3
5	lens matrices	4
5.1	Aperture Stop and Entrance Pupil	5
5.2	Exit Pupil and Pupil Matching	6
5.3	Vignetting	7
5.4	Aberrations	8
5.5	Field Curvature and Distortion	9
5.6	Chromatic Aberration	10
5.7	Coma and Astigmatism	11
5.8	Defocus and Spherical aberrations	12
6	Mechanical Design	14
6.1	Final Design Overview	15
7	Results and Discussion	16
8	Future Work	19
A	Doublet Lens	20
B	Eyepiece Lens	21
C	Code Listing	21
D	GitHub Repository	21
E	Doublet Lens Dispersion Properties	22

¹Thank you to Zemax, the staff who delivered the course on Optical Engineering on Coursera, Patrick for letting me use his workshop and helping me out in that regard, PVChaus for the PVC pipe and sawing, and the staff at the local library as well as the sponsors of the Imagine Space.

1 Summary

A telescope was designed as a learning experience. The hope of the designer was to gain some experience working on an optics project from start to finish. The author also intends to keep the finished piece as a decorative, yet functional spyglass. An inspiration for the project were the spyglass style optics used by sailors during centuries past, and fortunately these Galilean style looking glasses are reasonably priced and relatively simple.

2 Requirements

The requirements were not strict and are listed below:

- (a) Magnification of at least x 6, which is comparable to the angular magnification provided by binoculars.
- (b) A reasonably sized and positioned exit pupil.
- (c) Reduced chromatic aberration.
- (d) Readily portable.
- (e) upright image
- (f) examine a 2 meter object at 600 m (view across the Ottawa River to the West of downtown)

3 Materials

PLA 3D printing was chosen as the central solution for the mechanical design. Existing designs for DIY telescopes were also examined for inspiration. one notable such example is [1] which inspired the idea to use PVC pipe. A rack and pinion focuser was purchased online and parts were designed to fit with it and to connect it to the 3" PVC pipe. COTS lenses were purchased after being selected using Zemax optic Studio. Screws and heat-set threaded inserts were also used.

4 Optics

The design was completed using a combination of Zemax Optic Studio, MATLAB as well as pencil and paper. Lenses from various retailers were examined and it was decided that a doublet offered by Edmund Optics was the largest doublet that was within the budget of the project. The specifications are listed in Appendix A. A galilean style was chosen because it provides an upright image. However, what was designed is not a true Galilean telescope, because a doublet lens was used for the objective lens in order to improve the image quality.

4.1 Optic Studio Design

The two lens system was first designed in optic studio, primarily for the purpose of familiarization with the product. Many designs were tried before arriving at the single final design shown here. Only the lenses and placements were chosen in optic studio, and the performance of these items were evaluated in vacuum without consideration of the physical housing. Regardless, the trial license was expired by the time the mechanical housing was nearing a complete design.

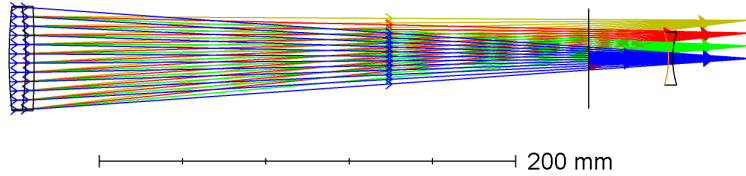


Figure 1: Cross Section of the optics layout, showing fields originating from 3 different angles.

	Surface Type	Comment	Radius	Thickness	Material	Coating	Clear Semi-Dia	Chip Zon	Mech Semi-Dia	Conic	TCE x 1E-6
0	OBJECT	Standard ▾	Infinity	Infinity			Infinity	0.000	Infinity	0.000	0.000
1	STOP (aper)	Standard ▾	45354	227.160	8.000	N-BAK4	EO_MGF2(550nm)	24.500 U	0.500	25.000	0.000
2	(aper)	Standard ▾	-174.830	4.000	N-SF10		24.500 U	0.500	25.000	0.000	-
3	(aper)	Standard ▾	-571.490	348.243		EO_MGF2(550nm)	24.500 U	0.500	25.000	0.000	0.000
4	Standard ▾	Infinity	-38.700	V			18.489	0.000	18.489	0.000	0.000
5	(aper)	Standard ▾	-61.530	2.000	S-BSL7		12.700 U	0.000	12.700	0.000	-
6	(aper)	Standard ▾	41.530	-40.386			12.700 U	0.000	12.700	0.000	0.000
7	IMAGE	Standard ▾	Infinity	-			23.894	0.000	23.894	0.000	0.000

Figure 2: Lens data for the lens layout shown in Fig. 2.

Later sections shall discuss the theoretical best performance of the system, as predicted by Optic Studio. It should be noted however that some of the Optic Studio Outputs were included in this report mainly as discussion points as well as something for the author to go back to for consultation. The individual subsections contain an indication of this when it was the case and it should be fairly obvious. Moreover, specific requirements regarding many of these outputs were never formulated, making it unnecessary and difficult to use these outputs as decision motivators in the design of the system.

5 lens matrices

$$\begin{bmatrix} y_o \\ \theta_o \end{bmatrix} = L_E T_{scope} L_F T_{gap} L_C \begin{bmatrix} y_i \\ \theta_i \end{bmatrix} \quad (1)$$

Where:

$$L_{doublet} = L_F T_{gap} L_C \quad (2)$$

$$L_C = \begin{bmatrix} 1 & 0 \\ (n_g - n_c)/R_{c1}n_g & n_c/n_g \end{bmatrix} \begin{bmatrix} 1 & d_c \\ 0 & 1 \end{bmatrix} \begin{bmatrix} 1 & 0 \\ (n_{air} - n_c)/R_{c2}n_{air} & n_c/n_{air} \end{bmatrix} \quad (3)$$

$$L_F = \begin{bmatrix} 1 & 0 \\ (n_{air} - n_f)/R_{f1}n_f & n_f/n_{air} \end{bmatrix} \begin{bmatrix} 1 & d_f \\ 0 & 1 \end{bmatrix} \begin{bmatrix} 1 & 0 \\ (n_f - n_g)/R_{f2}n_f & n_g/n_f \end{bmatrix} \quad (4)$$

$$T_{scope} = \begin{bmatrix} 1 & d_s \\ 0 & 1 \end{bmatrix} \quad (5)$$

$$T_{scope} = \begin{bmatrix} 1 & d_s \\ 0 & 1 \end{bmatrix} \quad (6)$$

$$L_E = \begin{bmatrix} 1 & 0 \\ (n_{air} - n_e)/R_{f1}n_f & n_e/n_{air} \end{bmatrix} \begin{bmatrix} 1 & d_e \\ 0 & 1 \end{bmatrix} \begin{bmatrix} 1 & 0 \\ (n_e - n_{air})/R_{e1}n_e & n_{air}/n_e \end{bmatrix} \quad (7)$$

Multiplying these together, we obtain the system matrix which is too large to include in this report. Substituting the numerical parameters of the system, we obtain the system matrix:

$$M = \begin{bmatrix} 0.4768 & 286.7697 \\ 0.0101 & 7.9592 \end{bmatrix} \quad (8)$$

Which corresponds closely to that of an afocal system with an angular magnification of ≈ 8 .

As a verification, the angular magnification obtained via the relation for thin lenses and using the effective focal lengths (in mm) of the lenses:

$$M_\theta = -\frac{f_e}{f_o} \quad (9)$$

$$= -\frac{350}{-39.7} \quad (10)$$

$$\approx 8.8161 \quad (11)$$

5.1 Aperture Stop and Entrance Pupil

For a telescope, the aperture stop corresponds to the Objective lens. For subsequent calculations, the aperture was chosen to correspond to 24.5 mm from the center of the front end (object side) of the objective lens. Indeed, the marginal ray for an object at infinity shall intercept the objective lens at the edge, and barring any other obstructions, shall make it through to the eyepiece. The aperture stop and entrance pupil for this system are expected to correspond approximately to the objective lens.

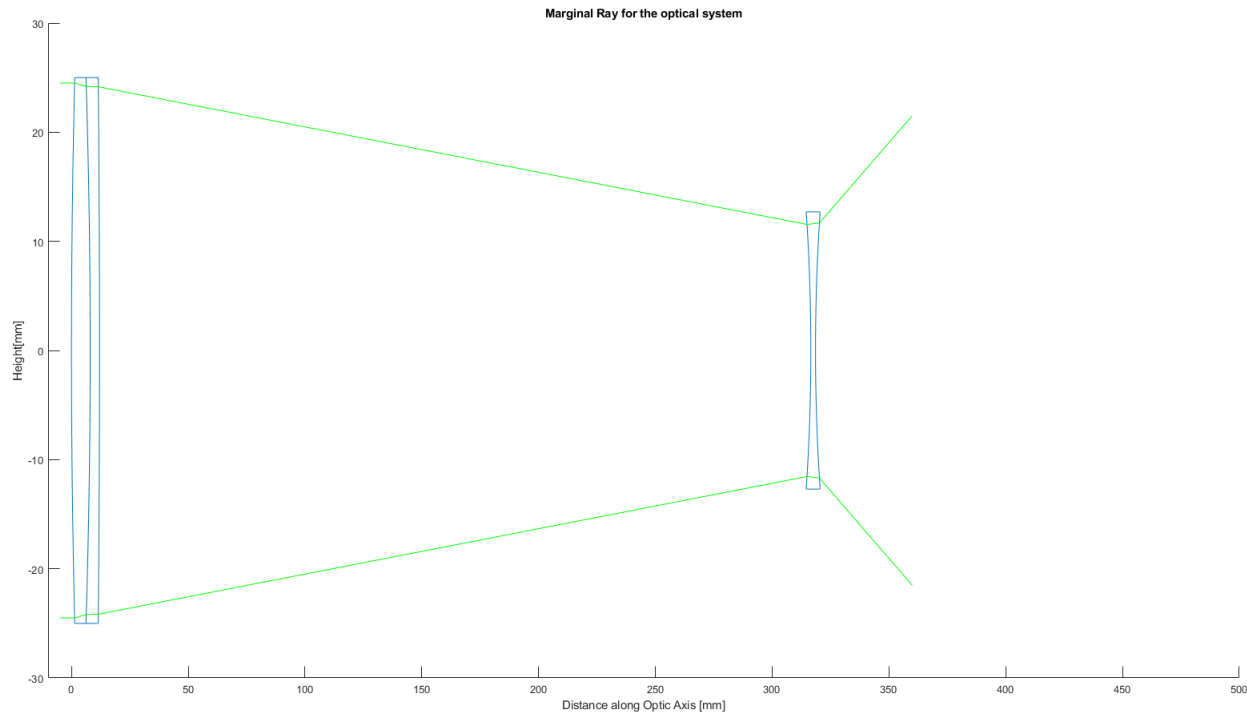


Figure 3: MatLab generated figured demonstrating marginal rays for the system.

5.2 Exit Pupil and Pupil Matching

The size of the exit pupil can be found by determining the size of the image of the entrance aperture. This can be found via ray tracing by extending multiple rays from a given height in the entrance aperture and finding the distance along the optical axis at which they intersect. The ray matrices for rays of height r_a and angles θ_i , originating from the upper edge of the entrance aperture, have the form:

$$T(-x)L_e T_{scope} \begin{bmatrix} r_a \\ \theta_i \end{bmatrix} \quad (12)$$

These rays are found to intersect at a distance of ≈ 36 mm, inside the system, measured from the image side face of the eyepiece lens. Propagating these rays backwards by this distance, we also find the height of the exit pupil, measured from the optical axis, to be ≈ 2.8 mm. Doubling this quantity we obtain 4.6 mm which satisfies the pupil matching requirement. The MATLAB code that was used to perform these calculations can be found in Appendix C. The size of the exit pupil can also be estimated using the angular magnification of the system [2]:

$$D_{ex} = \frac{D_{obj}}{M} \quad (13)$$

$$\approx 5.5580 \text{ mm} \quad (14)$$

which is suitable for viewing with the human eye for which the pupil varies between 2 and 8 mm. The disagreement between results may be due to the fact that this formula was derived for a system of thin lenses.

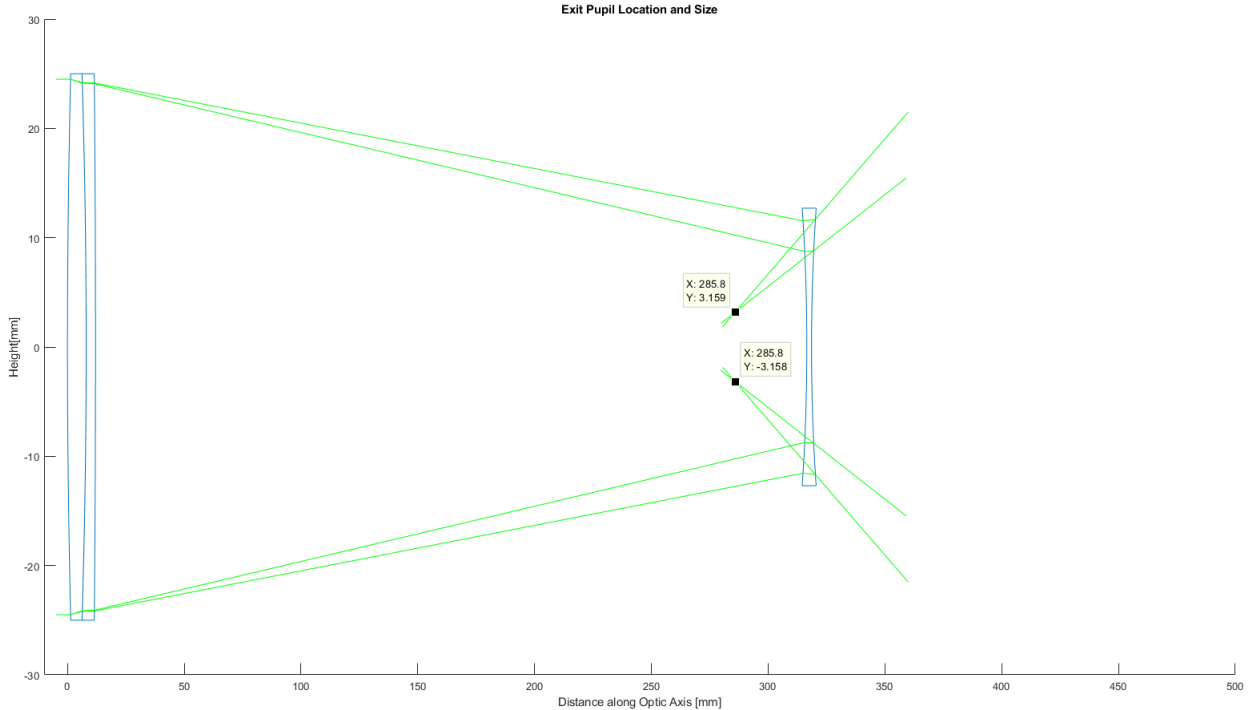


Figure 4: A graphical estimation yields an estimate of ≈ 6.4 mm and a location of ≈ 31 mm to the left of the inner edge of the eyepiece.

The exit pupil that was estimated in OpticStudio was 5.55 mm, which can be seen in some of the captions of figures included in this report.

5.3 Vignetting

In a vaccuum, the eyepiece lens acts as the field stop of the system. Optic studio was used to predict vignetting for fields incident on the entrance aperture at 1, 2 and 3 degrees. The results are shown in Fig. 5

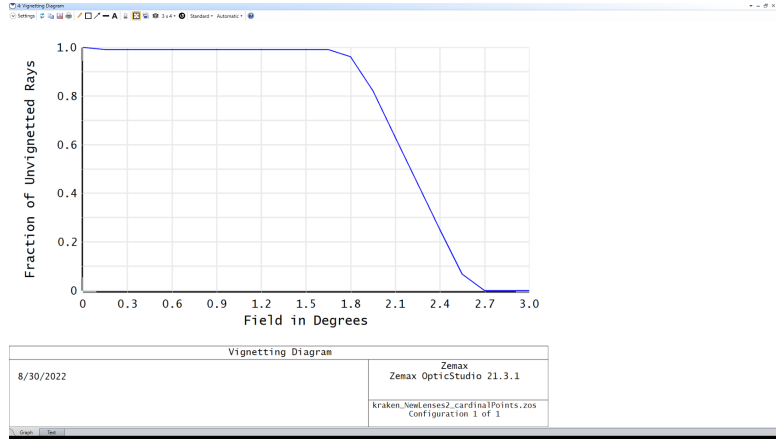


Figure 5: Optic Studio generated vignetting plot.

A total vignetted field of view of just under 5 degrees was deemed adequate. For example, a 2 m object 800 m away occupies only ≈ 0.2 degrees and at 8x magnification, ≈ 1.5 degrees, which falls well within the region of only very small vignetting. It is also reassuring that this field of view is also similar to binoculars [3] or spotting scopes [4].

As a learning exercise, vignetting calculations were also performed in Matlab to determine at which angle incoming rays would not make it into the eyepiece. The results are shown in Fig. 6.

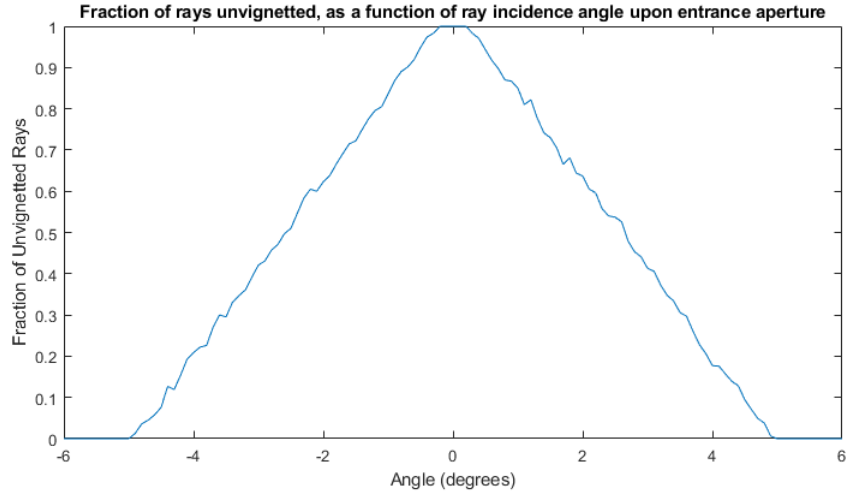


Figure 6: Results of a Monte Carlo simulation for ray incidence angles between -6 and 6 degrees, with 1000 trials per angle. Height in aperture was sampled from a uniform distribution. Error bars were deemed unnecessary for the purpose of this plot.

Comparing Figs. 6 and 5 we see disagreement between the results. It is not clear what the cause of the difference is and at this time, the author is not well versed in the existing literature on computation of vignetting. The maximum angle ray used in Optic Studio was 3 degrees and the vignetting simulation may have used a fitting algorithm that set it to 0 above that, which could have affected other numbers, but this is speculation.

5.4 Aberrations

With the double convex lens as the eyepiece, it was expected that there would be significant distortion. This was confirmed by the Seidel Sum diagram generated by OpticStudio.

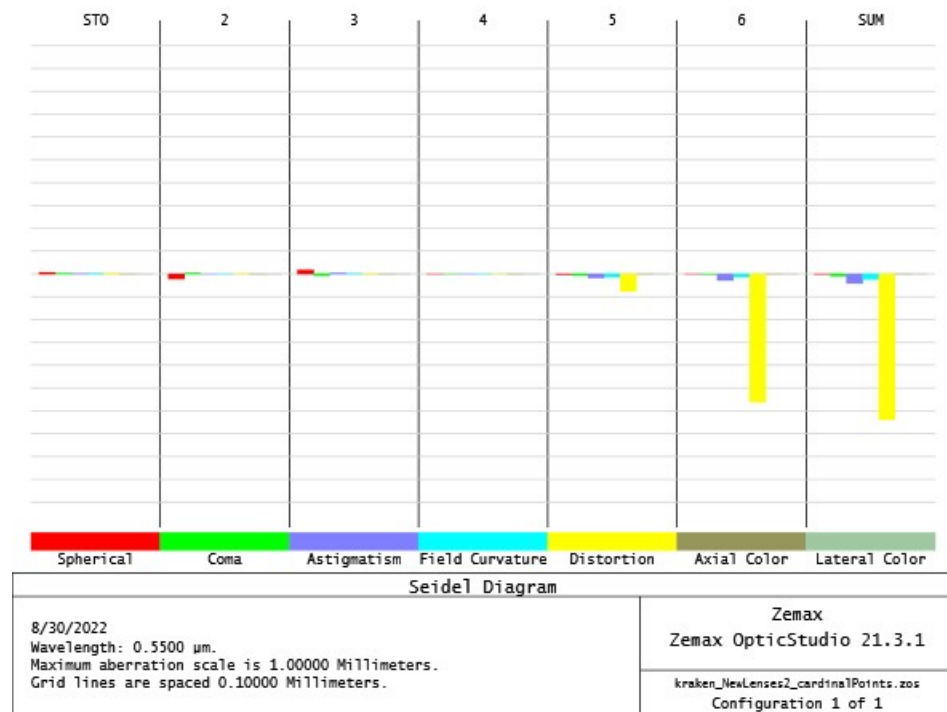


Figure 7: The aberrations are expected to be dominated by Distortion

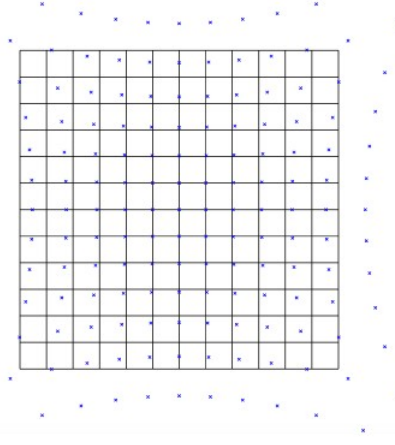
This information, along with the image simulation and vignetting plot were the principal Optic Studio outputs, other than the component diagram, that were used to justify moving forward with construction. At this time, it is unclear to the author what could serve as a quantified system requirement.

5.5 Field Curvature and Distortion

Given that the distortion appears to be worse towards the edge of the image, as evidence by the image simulation shown in Fig. 8a and that objects under observation would occupy significantly less than this total space, these results were deemed adequate and expected. In other words, the worst source of aberration is expected to be mitigated by the restricted field of view.



(a) Image simulation for a 2.5 degree object height.



(b) Grid distortion for a 4.2466 degree field @ 0.055 μ m. Maximum distortion was 55.3126%.

Figure 8: OpticStudio Outputs demonstrating aberrations. The image in the centers appears quite good, while the edges are blurred and distorted.

Optic Studio also generated the figure shown in Fig. 9.

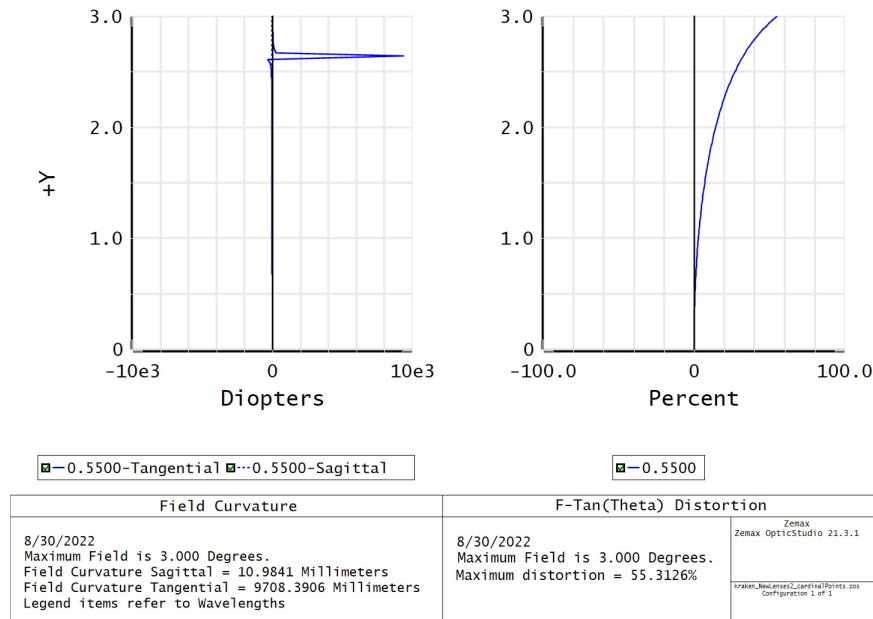


Figure 9: Figures showing the amount of distortion present from 0 to 3 degrees.

5.6 Chromatic Aberration

Chromatic aberration is mitigated by the doublet lens that is used as the objective lens. This lens uses a flint glass that brings the wavelengths separated by the crown lens back into focus. Appendix E shows the spot diagram, focal shift, ray fan plot and polychromatic diffraction MTF as a function of wavelength for the doublet, however no specific requirements exist for this system, other than it be useable. It was assumed, given the high quality of the lens and it's specified operational range that it would be adequate for this project. It would have been useful as an academic exercise to examine the longitudinal aberration plot in optic Studio, to see where the focus lies as a function of wavelength for the total system, in order to see a visualization of the aberration of the total system.

5.7 Coma and Astigmatism

Coma primarily affects the imaging of far off axis objects and was not expected to significantly affect the performance of this device. Furthermore, there were no requirements regarding off-axis imaging, other than the system must be “usable”. Optic studio does predict some coma for off-axis images and the result is shown in Fig. 10.

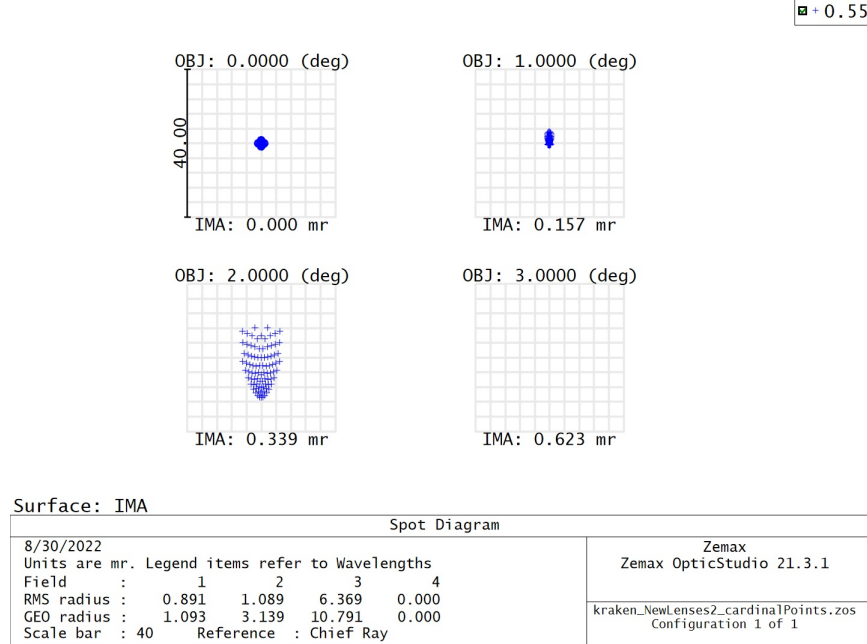


Figure 10: Spot diagram showing high coma for off axis objects.

Indeed, coma appears to dominate the transverse ray fan plots at non-zero angles of incidence (Fig. 11).

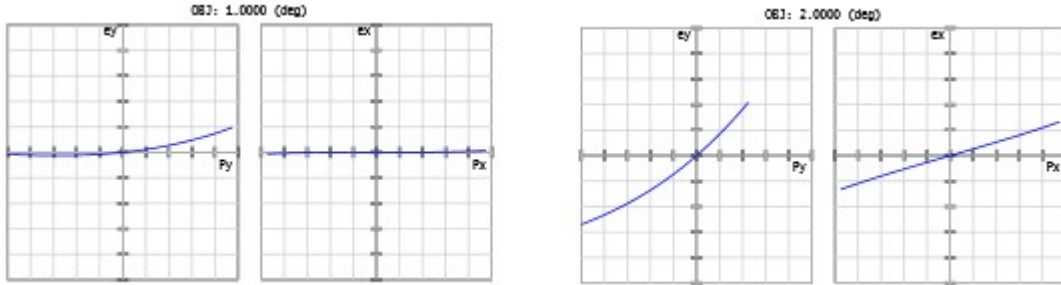


Figure 11: Note the approximately quadratic dependence of the ray fan in the left diagrams for each field.

Due to the symmetry of the system, astigmatism was not expected. However, The seidel diagram as well as the ray fan plots indicate that some astigmatism is to be expected.

5.8 Defocus and Spherical aberrations

From the “Through Focus Spot diagram” shown in Fig. 12, we can see that at small angles of incidence and defocus the performance should be good. Whereas at larger angles of incidence there is either large coma or the rays do not make it through the system.

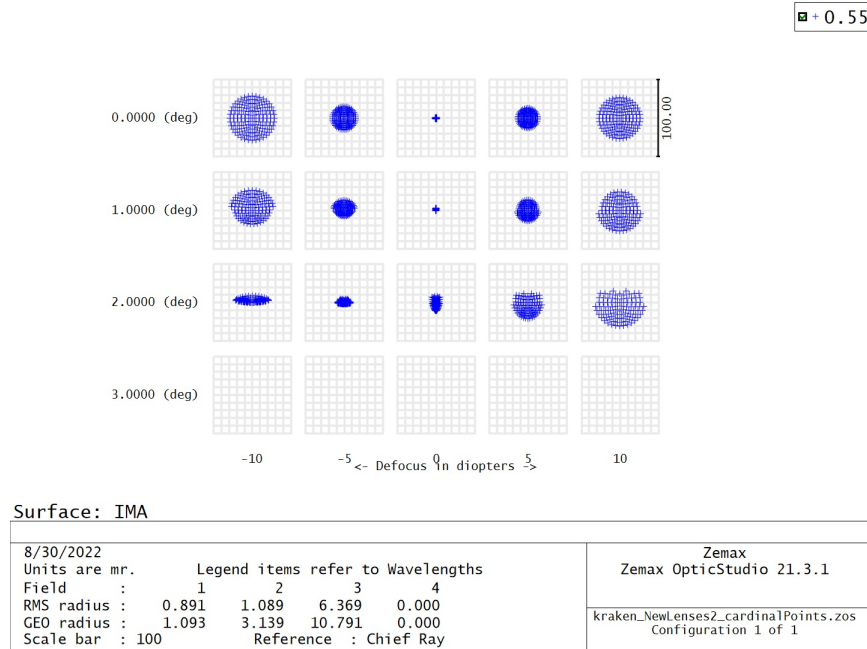


Figure 12

In Fig. 13 we see that small spherical aberrations (cubic radial dependence) dominate the aberrations for rays with 0 degree incidence. Other angles of incidence are not shown, because they are not dominated by spherical aberration.

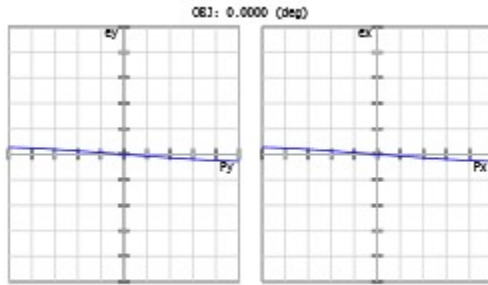
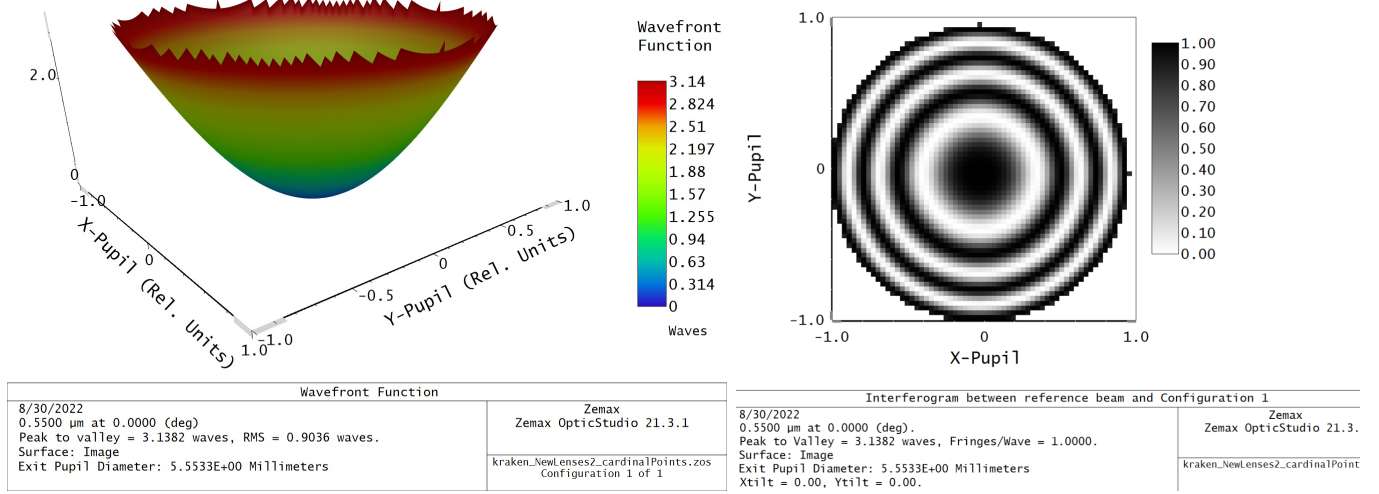


Figure 13: Maximum scale ± 20 mr, for an exit pupil diameter of 0.550

The wavefront aberration plot appears to be dominated by defocus, which is shown in Fig. 14a. It appears that at a field angle of 0, because the distortion is very small that the aberrations in the image are dominated by defocus. However, given that this defocus should be entirely correctable by moving the eyepiece position relative to the objective, it was deemed to not be particularly useful information. The same goes for the interferogram (Fig. 14b), which also appears to indicate that defocus is the primary aberration.



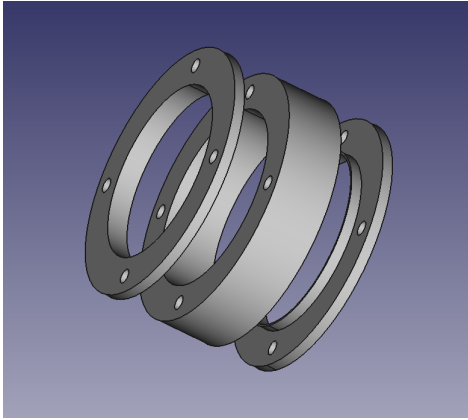
(a) Wavefront Map generated in OpticStudio.

(b) Interferogram generated in OpticStudio.

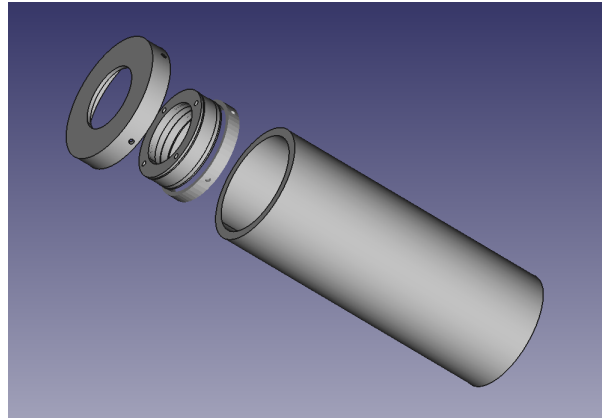
Figure 14: OpticStudio Outputs demonstrating aberrations at 0 incidence angle.

6 Mechanical Design

The objective lens sits in a ring and held in place by two identical lenscaps. All stl files found on github, the link for which is provided in Appendix D.



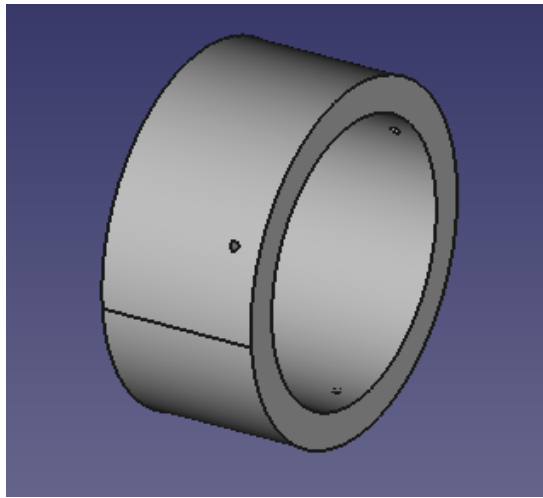
(a) Exploded view of the Objective Lens holder.



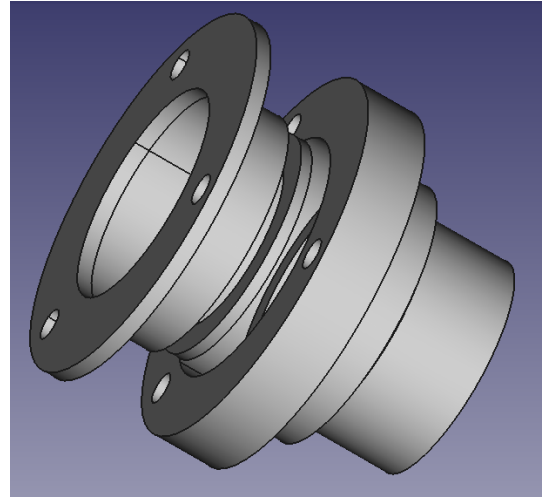
(b) Objective lens holder position within the head.

Figure 15: FreeCad diagrams of some more of the 3D printed pieces.

The PVC pipe was sanded and painted with a Matte black, the exterior was coated with a transparent layer. A rack and pinion (RnP) focusing system was purchased online as a body that connects the PVC pipe to the eyepiece and allows for some motion between the eyepiece and objective, to account for small errors in the build and calculations. A part was 3D printed to fit and connect the PVC pipe to the RnP (Fig. 16a). Pilot holes were printed at angles of 120° to the bottom hole, centered on the vertical axis, so that holes could be easily drilled to align with the small holes that came stock with the RnP mount. Its place in the assembled scope is shown in Fig. 17.



(a) RnP to PVC adapter. Holes were also drilled on the other end of the fitting to connect it to the PVC pipe.



(b) Exploded view of the eyepiece holder assembly. Additional holes were drilled in the eyepiece holder.

Figure 16: FreeCad diagrams of some more of the 3D printed pieces. Holes were drilled in, rather than printed in, in some cases, in order to make things easier to line up.

A hole was also drilled in the PVC pipe so that a tripod can be connected to the pvc via a 1/4" diameter threading. This piece is not shown due to the fact that it necessitates a re-design. More on this in a later section.

6.1 Final Design Overview

The location of each component in the final product are listed below in reference to Fig 17 and the “final” construction is shown in Fig. 18.

- (a) Cap holding the lens in place. This lens caps features internal ridges that hold the objective lens holder in place.
- (b) Objective Lens Assembly (Fig. 15a sits within the PVC pipe).
- (c) Internal Objective Lens Holder.
- (d) Flush Mount (note: requires redesign)
- (e) Rack and Pinion to PVC adapter. Note that the additional drill holes to connect the piece to the PVC pipe are not shown.
- (f) Eyepiece assembly (Fig. 16b)

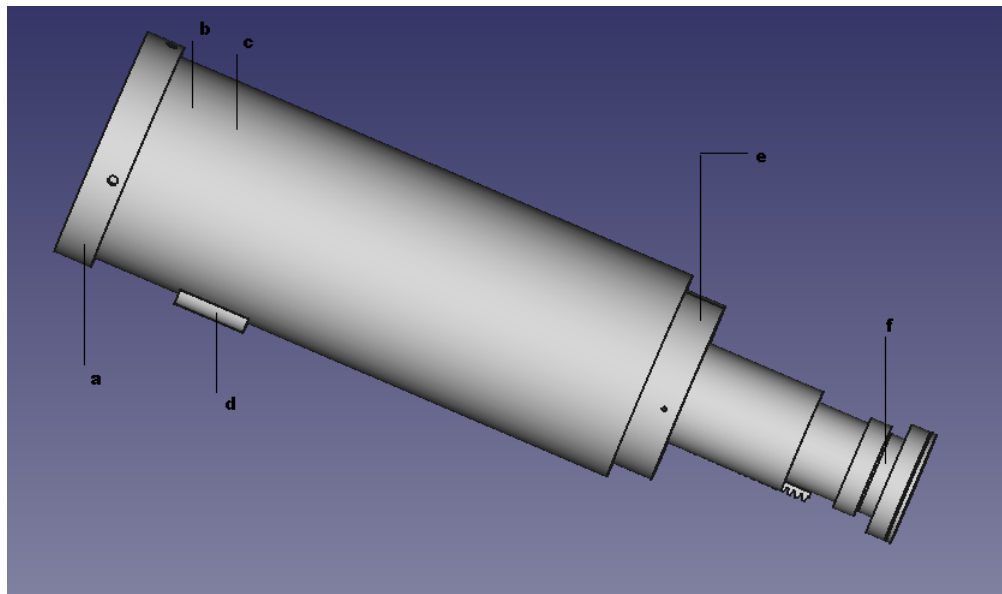


Figure 17: FreeCad diagram with all components fit together in order to show the final design.

7 Results and Discussion

The initial fully constructed telescope is shown in Fig. 18. The scope is usable and functional. the project can be deemed a success, however there are some things that could be done better. This is discussed in the following sections.



Figure 18: Initial construction.

The goal, or hope, when conceptualizing the initial design was to create a mechanical body for the telescope which did not change the theoretical analysis. In the purely optical design, the field stop corresponded to the eyepiece lens. Unfortunately, the rack and pinion system included multiple unexpected stops within the body. Furthermore the rack system was quite long and had to be shortened by sawing off the end and unfortunately it is still quite long. This Field stop is also likely not located exactly in the virtual image plane. Shown in Fig. 19 are the approximate effects of the two stops “imposed” on the design. The first stop indicates the edge of the inner moveable tube of the rack and pinion system, the second is another stop that is located within the tube and is clearly the most egregious offender on the FoV of the system. The rearmost stops located to the right of the eyepiece are the possible stops imposed by the 3D printed component shown in Fig. 16b.

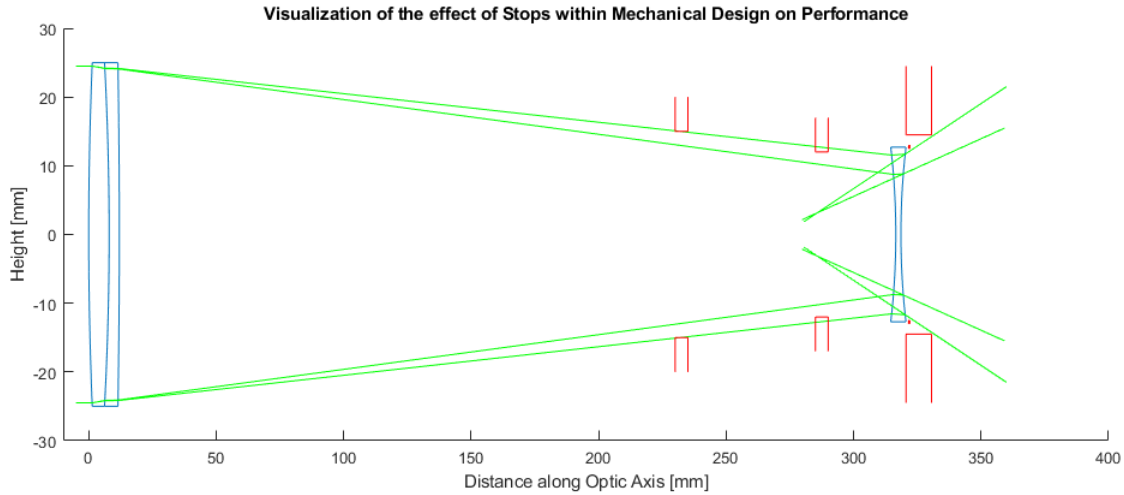


Figure 19: Diagram showing additional possible fieldstops.

It proved to be incredibly difficult to take an image through the spyglass and Fig. 20, an image of some trees viewed across the Ottawa river, West of downtown will have to suffice for the time being.



Figure 20: Highest quality photo taken through the device (to date). Some digital magnification had to be used in order to get the exit pupil to occupy the field of view of the cell-phone camera.

It would be ideal to design or purchase a larger focuser that would not constrain the system beyond the theoretical design. This design flaw highlights the value of a prototyping phase in the design. An optics workbench could have served this role as a prototyping environment, however this was not an option and building a setup would have taken considerable time. Access to a 3D printer was also highly restricted; the 3D printer at the library could only be booked for 2 hours at a time, a maximum of 4 times per month, which greatly limited the amount of prototyping that could be done. This made printing accessories and other prototypes relatively difficult and the possibility of 3D printing some mounts for testing was not pursued.

During testing of the device, it was noticed that when the rack and pinion was fully extended, some objects within 10 meters were imaged quite sharply. It was then discovered with some testing that the system also served as an magnifier at close ranges.

Some “lessons learned” are listed point form below:

- More time inspecting existing telescope design could have led to a better final “product” without substantial time investment. For example, a brass insert was used directly in the scope siding, whereas profession scopes using a rounded fitting that allows for easy adjustment of the location. The insert was also incredibly difficult to put into the hole that was drilled for it and would require specialized tools. It would have been much easier to insert this into PLA, which would then be secured to the tube in the way that is standard for this style of telescope.
- The 3D printer appeared to not always print as expected, resulting in some failed prints and components that did not quite fit. Overall
- Ended up having to repaint due to damage occurring during the drilling of the holes. Still do not have a solution for chip proof coating.
- 3 Screws are more stable than 4
- The design of the physical components took quite some time and unfortunately, the full mechanical body could not be simulated in OpticStudio.
- Paid a lot of money for glue and a UV flashlight to cure it, but this ended up being unnecessary and messy, the lens caps did a fine job of holding the lens in place.
- The tripod extension was originally intended as a hand-grip, but in hindsight, it would have been nice to be able to use it as a functional tripod as well, unfortunately the design does not allow vertical tilting, which makes it a rather ineffective tripod.
- Project took substantially longer than expected.

8 Future Work

Some future work may involve:

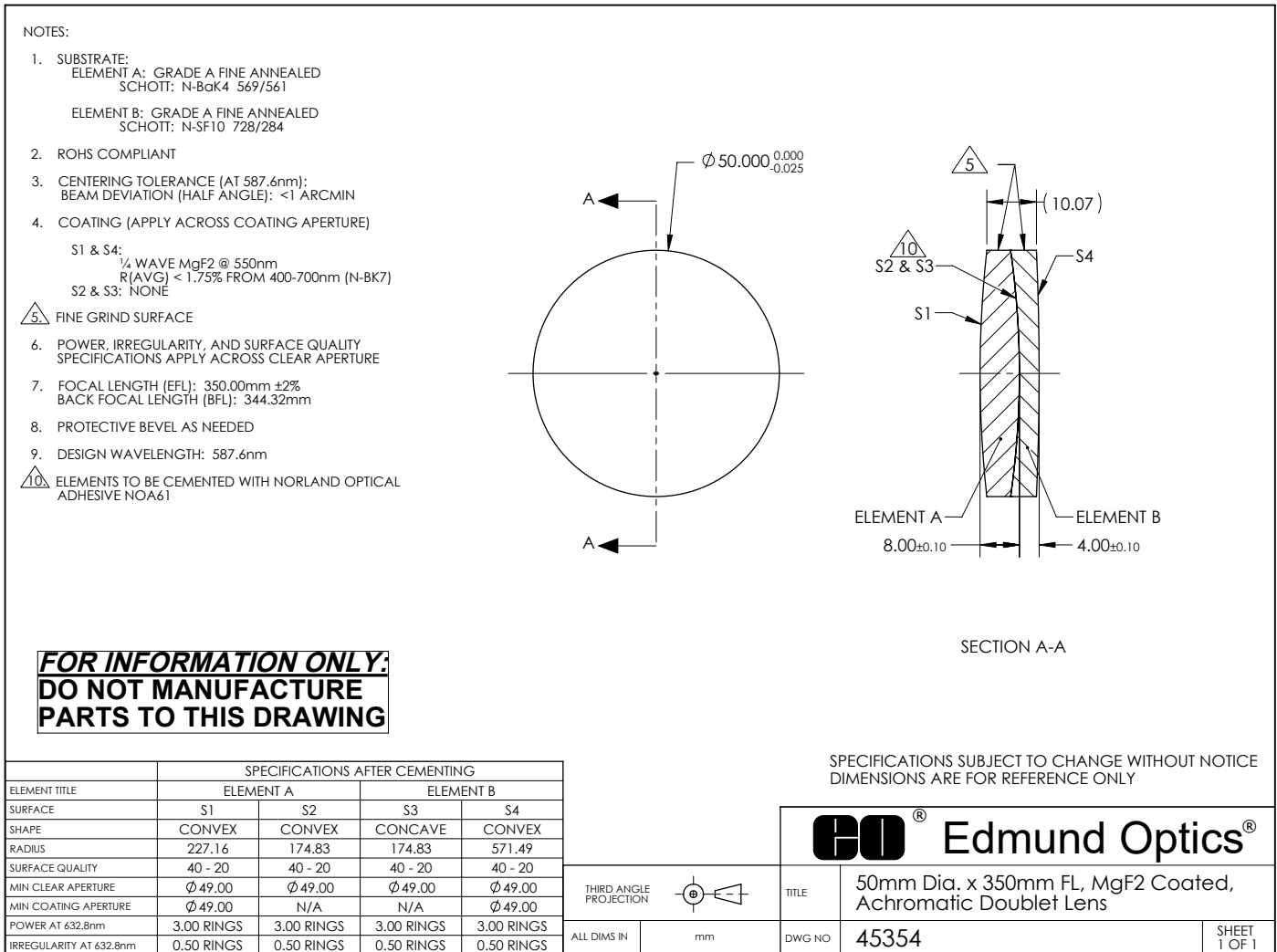
- Quantifying aberrations and translating to requirements.
- Study on performance metrics.
- Mount the optic components to a workbench in order to perform measurements.

At this time, these are not priorities. Instead, more time shall be spent studying theory in order to gain a more intuitive understanding of many of the concepts explored in this document.

References

- [1] <https://www.youtube.com/watch?v=deUJ1M6ew0Y&list=PL3MWXRq-wTfGeGKto1UZ-lgpb4CBKFA4W&index=15&t=167s>
- [2] Pedrotti, "Introduction to Optics", Third Edition, Pearson.
- [3] <https://www.crutchfield.com/S-9L0h4V1C5l5/learn/binoculars-buying-guide.htm>
- [4] <https://www.optics-trade.eu/blog/field-of-view-calculations/>

A Doublet Lens



B Eyepiece Lens

	Beamsplitters										
	Polarizers										
	Lenses										
	Multi-Element Optics										
	Filters										
	Prisms										
	Substrates/Windows										
	Optical Data										
SLB-25B-60N	M	IR1	IR2	$\phi 25$	-59.7	4.5	2.0	-60.3	62.28	<1	
SLB-25B-70N	M	IR1	IR2	$\phi 25$	-69.7	4.2	2.0	-70.3	72.66	<1	
SLB-25B-80N	M	IR1	IR2	$\phi 25$	-79.7	4.0	2.0	-80.3	83.04	<1	
SLB-25B-100N	M	IR1	IR2	$\phi 25$	-99.7	3.5	2.0	-100.3	103.80	<1	
SLB-25.4B-25N	M	IR1	IR2	$\phi 25.4$	-24.7	8.6	2.0	-25.4	25.95	<1	
SLB-25.4B-30N	M	IR1	IR2	$\phi 25.4$	-29.7	7.4	2.0	-30.4	31.14	<1	
SLB-25.4B-40N	M	IR1	IR2	$\phi 25.4$	-39.7	6.0	2.0	-40.4	41.52	<1	
SLB-25.4B-50N	M	IR1	IR2	$\phi 25.4$	-49.7	5.2	2.0	-50.4	51.90	<1	
SLB-25.4B-60N	M	IR1	IR2	$\phi 25.4$	-59.7	4.6	2.0	-60.4	62.28	<1	
SLB-25.4B-70N	M	IR1	IR2	$\phi 25.4$	-69.7	4.2	2.0	-70.4	72.66	<1	
SLB-25.4B-80N	M	IR1	IR2	$\phi 25.4$	-79.7	4.0	2.0	-80.4	83.04	<1	
SLB-25.4B-100N	M	IR1	IR2	$\phi 25.4$	-99.7	3.6	2.0	-100.4	103.80	<1	
SLB-25.4B-150N	M	IR1	IR2	$\phi 25.4$	-149.7	3.0	2.0	-150.4	155.70	<1	

C Code Listing

See github page for additional code. only a sample is shown:

```
% Determine transformation of ray through system and eyepiece
Ep(:,1) = Reye*Tm*Ld*Td*Lo*[24.5;0]
Ep(:,2) =Reye*Tm*Ld*Td*Lo*[24.5;4.0833e-05]
Ep(:,3) =Reye*Tm*Ld*Td*Lo*[24.5;0.01]
Ep(:,4) =Reye*Tm*Ld*Td*Lo*[24.5;0.02]

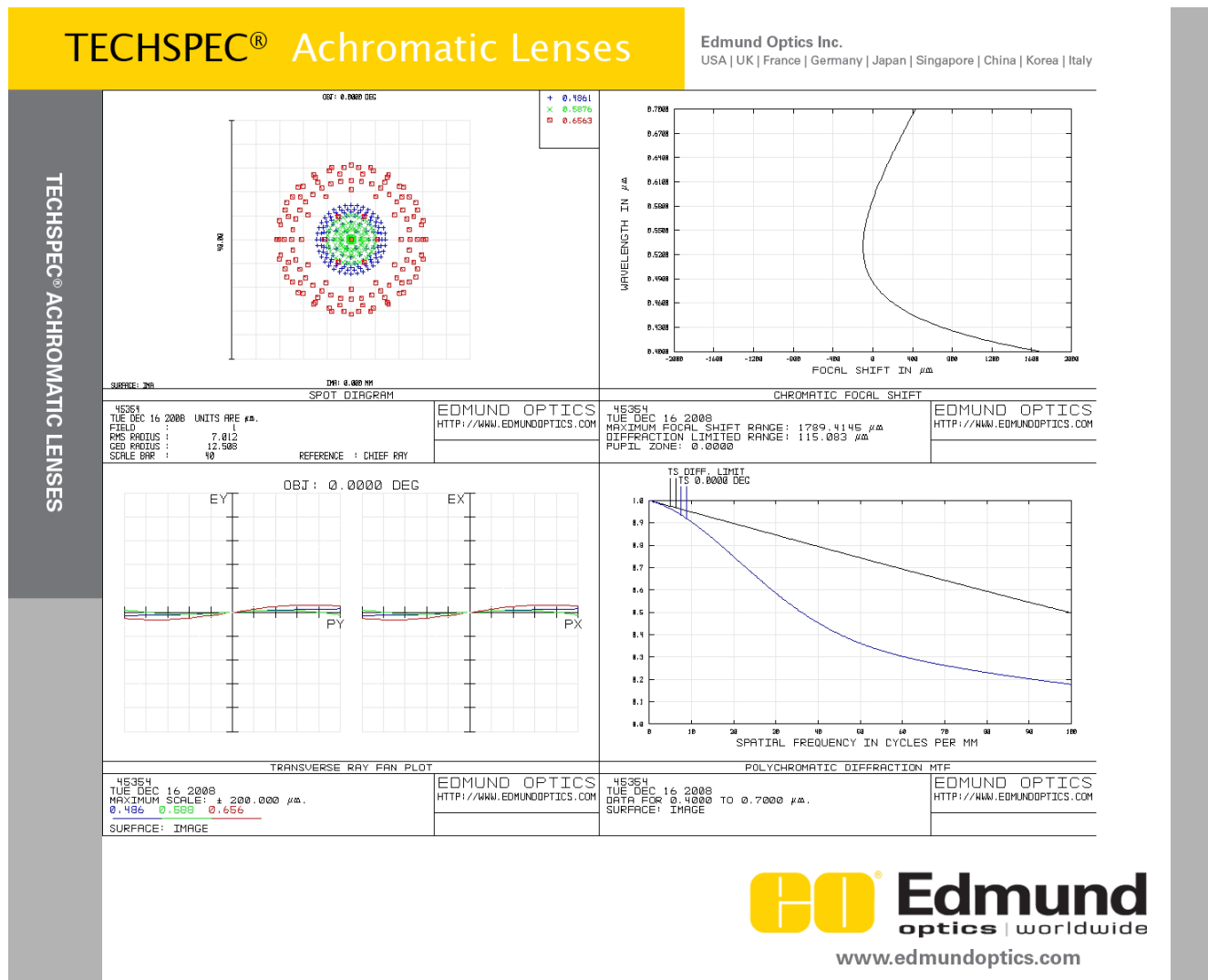
%find location at which the rays intersect
(Ep(1,1)-Ep(1,2))/(Ep(2,1)-Ep(2,2))
(Ep(1,2)-Ep(1,3))/(Ep(2,2)-Ep(2,3))
(Ep(1,3)-Ep(1,4))/(Ep(2,3)-Ep(2,4))

%translate backwards by this distance
T(-(Ep(1,1)-Ep(1,2))/(Ep(2,1)-Ep(2,2)))*Reye*Tm*Ld*Td*Lo*[24.5;0]
T(-(Ep(1,1)-Ep(1,2))/(Ep(2,1)-Ep(2,2)))*Reye*Tm*Ld*Td*Lo*[24.5;4.0833e-05]
```

D GitHub Repository

The github repository for the project can be found at <https://github.com/Jewels-1/spyglass.git>

E Doublet Lens Dispersion Properties



Edmund
optics | worldwide
www.edmundoptics.com